

Equilibrium statistics of an inelastically bouncing ball, subject to gravity and a random force

Theodore W. Burkhardt¹ and Stanislav N. Kotsev^{1,2}

¹*Department of Physics, Temple University, Philadelphia, PA 19122*

²*Department of Chemistry, Rice University, Houston, TX 77005*

(Dated: March 23, 2022)

We consider a particle moving on the half line $x > 0$ and subject to a constant force in the $-x$ direction plus a delta-correlated random force. At $x = 0$ the particle is reflected inelastically. The velocities just after and before reflection satisfy $v_f = -rv_i$, where r is the coefficient of restitution. This simple model is of interest in connection with studies of driven granular matter in a gravitational field. With an exact analytical approach and simulations we study the steady state distribution function $P(x, v)$.

I. INTRODUCTION

Consider a particle moving on the half line $x > 0$ and subject to a constant force in the $-x$ direction, such as gravity, and an additional delta-correlated random force with zero mean. The Newtonian equation of motion has the form

$$\frac{d^2x}{dt^2} = -g + \eta(t), \quad \langle \eta(t)\eta(t') \rangle = 2\Lambda\delta(t-t'), \quad (1)$$

where g is a positive constant. With no loss of generality we set $g = 1$, $\Lambda = 1$ throughout this paper, since this can be achieved by rescaling [1] of x and t . At the boundary $x = 0$ the particle is reflected inelastically. The velocities just after and before reflection satisfy

$$v_f = -rv_i, \quad (2)$$

where r is the coefficient of restitution. The simple model defined by Eqs. (1) and (2) is of interest in connection with driven granular gases, see, e.g., [2]. Cornell, Swift, and Bray [3] originally proposed the model and studied the case $g = 0$.

According to Eq. (1) the mean energy $E(t) = \langle \frac{1}{2}v(t)^2 + x(t) \rangle$ of the randomly accelerated particle at time t increases as $E(t) = E(0) + t$ between boundary collisions but decreases, for $r < 1$, in the collisions. Eventually an equilibrium is reached. In this paper we study the equilibrium distribution function $P(x, v)$ with an exact analytical approach and simulations. In related earlier work, but without gravity, we have considered (i) the equilibrium of a randomly accelerated particle moving on the finite line between two inelastically reflecting boundaries [4, 5], and (ii) non-equilibrium properties of a randomly accelerated particle on the half line [6, 7] and on the finite line [8] for absorbing, partially absorbing, and inelastic boundary conditions.

The equilibrium distribution function $P(x, v)$ of a particle, which moves according to Eq. (1) for $x > 0$ and is reflected inelastically at $x = 0$, satisfies the steady-state Fokker-Planck equation [9]

$$\left(v \frac{\partial}{\partial x} - \frac{\partial}{\partial v} - \frac{\partial^2}{\partial v^2} \right) P(x, v) = 0, \quad (3)$$

with the boundary condition

$$P(0, -v) = r^2 P(0, rv) \quad , \quad v > 0. \quad (4)$$

The factors of r in Eq. (4) take the change in velocity (2) into account and ensure that the incident and reflected probability currents at the boundary have equal magnitude

$$I = \int_0^\infty dv v P(0, -v) = \int_0^\infty dv v P(0, v) . \quad (5)$$

Here we have assumed the standard normalization,

$$\int_0^\infty dx \int_{-\infty}^\infty dv P(x, v) = 1 , \quad (6)$$

of the distribution function.

The main goal of the paper is to solve the steady-state Fokker-Planck equation (3) with boundary condition (4). In Section II we derive an integral equation for the distribution function $P(0, v)$ at the boundary and show how to obtain $P(x, v)$ from $P(0, v)$ by integration. In Section III the asymptotic form of $P(0, v)$ for large and small v is determined, for arbitrary r , from the integral equation. For two particular values, $r = \frac{1}{2}$ and $\frac{1}{3}$, the integral equation is solved exactly and the corresponding $P(x, v)$ obtained by integration. We have also carried out numerical simulations of the randomly accelerated particle in a gravitational field. The algorithm is described in Section IV, and the results of the simulations are compared with our analytic predictions. Section V contains closing remarks.

II. INTEGRAL EQUATION FOR $P(x, v)$

The Fokker-Planck equation (3) is readily solved by separation of variables. The most general solution which vanishes for $x \rightarrow \infty$ and $v \rightarrow \pm\infty$ is given by [6]

$$P(x, v) = e^{-v/2} \int_0^\infty dF w(F) e^{-Fx} \psi_{1/4, F}(-v) , \quad (7)$$

where $w(F)$ is an arbitrary function, and $\psi_{s, F}(v)$, with $F > 0$, is the solution of the ordinary differential equation

$$\left(-\frac{d^2}{dv^2} + Fv + s \right) \psi_{s, F}(v) = 0 \quad (8)$$

which vanishes for $v \rightarrow \pm\infty$. This solution is given by

$$\psi_{s, F}(v) = F^{-1/6} \text{Ai} \left(F^{1/3} v + F^{-2/3} s \right) , \quad (9)$$

where $\text{Ai}(z)$ is the standard Airy function [10]. Normalized as in Eq. (9), the $\psi_{s, F}(v)$ have the orthogonality and closure properties [6]

$$\int_{-\infty}^\infty dv v \psi_{s, F}(\pm v) \psi_{s, G}(-v) = \begin{cases} 0 , & \text{upper sign} \\ \delta(F - G) , & \text{lower sign} \end{cases} \quad (10)$$

$$\int_0^\infty dF [\psi_{s,F}(-v)\psi_{s,F}(-u) - \psi_{s,F}(v)\psi_{s,F}(u)] = v^{-1}\delta(v-u) . \quad (11)$$

Making use of Eqs. (7), (9), and the relation $\int_{-\infty}^\infty dt e^{-at} \text{Ai}(-t) = \exp(a^3/3)$ for $a > 0$, one finds that the probability density $P(x)$ for the position of the particle is given by

$$P(x) = \int_{-\infty}^\infty dv P(x, v) = \int_0^\infty dF F^{-1/2} w(F) \exp[-(12F)^{-1} - Fx] , \quad (12)$$

and that the normalization condition (6) is satisfied if

$$\int_0^\infty dx P(x) = \int_0^\infty dF F^{-3/2} w(F) \exp[-(12F)^{-1}] = 1 . \quad (13)$$

To invert Eq. (7), it is convenient to use the auxiliary functions [6]

$$\phi_{s,F}(v) = \psi_{s,F}(v) - \int_0^\infty \frac{dG}{2\pi} \frac{\exp[-\frac{2}{3}s^{3/2}(F^{-1} + G^{-1})]}{F + G} \psi_{s,G}(-v) , \quad (14)$$

which vanish for $v > 0$ and have the biorthogonality property

$$\int_0^\infty dv v \phi_{s,F}(-v) \psi_{s,G}(-v) = \delta(F - G) \quad (15)$$

on the semi-infinite interval $v > 0$. Functions of this type were first constructed by Marshall and Watson [11] and exploited in [6, 11, 12] in calculating first passage properties.

Using property (15) to solve Eq. (7) for $w(F)$, we obtain

$$w(F) = \int_0^\infty dv v \phi_{1/4,F}(-v) e^{v/2} P(0, v) . \quad (16)$$

Substituting this result back in Eq. (7) and imposing the boundary condition (4) leads to

$$r^2 P(0, rv) = \int_0^\infty du u G_g(v, u) P(0, u) , \quad (17)$$

$$G_g(v, u) = e^{(v+u)/2} \int_0^\infty dF \psi_{1/4,F}(v) \phi_{1/4,F}(-u) . \quad (18)$$

Equations (7) and (16)-(18) provide us with a strategy for calculating $P(x, v)$. First $P(0, v)$ is determined by solving the integral equation (17). Then $w(F)$ and $P(x, v)$ are obtained by evaluating the integrals in Eqs. (16) and (7), respectively.

The kernel in integral equation (17) has a simple physical interpretation. The quantity $v G_g(v, u) dv$ is the probability that a particle moving according to Eq. (1) with initial position $x = 0$ and initial velocity $u > 0$ arrives with speed between v and $v + dv$ on its first return to $x = 0$. Integral equation (17) for the equilibrium distribution follows immediately from

this interpretation. For consistency with the probabilistic interpretation, $G_g(v, u)$ should be symmetric in v and u and normalized so that

$$\int_0^\infty dv v G_g(v, u) = 1. \quad (19)$$

That the expression for $G_g(v, u)$ in Eq. (18) satisfies both these conditions can be shown with the help of Eqs. (9), (11), and (14).

The integral representation of $G_g(v, u)$ in Eqs. (18) is useful because of the simple orthogonality and closure properties of the basis functions. Two other useful representations,

$$G_g(v, u) = \frac{e^{(v+u)/2}}{\pi^2 v u} \int_0^\infty d\gamma \gamma \frac{\sinh(\pi\gamma)}{\cosh(\pi\gamma/3)} K_{i\gamma}(v) K_{i\gamma}(u) \quad (20)$$

$$G_g(v, u) = \frac{3}{2\pi} (vu)^{1/2} e^{(v+u)/2} \int_0^1 dy \left\{ \exp \left[-(v^2 - vu + u^2 + 3vuy^2)^{1/2} \right] \right. \\ \left. \times \left[(v^2 - vu + u^2 + 3vuy^2)^{-3/2} + (v^2 - vu + u^2 + 3vuy^2)^{-1} \right] \right\}, \quad (21)$$

follow from a classic paper of McKean [13], as shown in Appendix A. In Eq. (20), $K_\nu(z)$ is the standard modified Bessel function [10, 14]. Expressions (20) and (21) are particularly convenient for analytical (see Appendix B) and numerical calculations, respectively.

III. SOLUTION OF INTEGRAL EQUATION (17)

A. Asymptotic form of $P(0, v)$ for small v

First we derive the asymptotic form of $P(0, v)$ for small and large v from integral equation (17). Using representation (21) for the kernel, one finds that the ansatz

$$P(0, v) \sim v^{-\beta(r)}, \quad v \searrow 0 \quad (22)$$

is consistent with the integral equation if the exponent $\beta(r)$ satisfies

$$r = \left[2 \sin \left(\frac{2\beta + 1}{6} \pi \right) \right]^{1/(\beta-2)}. \quad (23)$$

The dependence of β on the coefficient of restitution r is shown in Fig. 1. As r decreases from 1 to 0, $\beta(r)$ increases monotonically from 0 to 5/2. The probability density for finding the particle at the boundary with velocity v diverges as v approaches zero, and the greater the inelasticity, the stronger the divergence.

The exponent β has the value 2 at

$$r_c = e^{-\pi/\sqrt{3}} = 0.163 \dots \quad (24)$$

For $r < r_c$, $\beta(r) > 2$, so that $P(0, v)$ diverges more strongly than v^{-2} in the limit $v \searrow 0$. Thus, for $r < r_c$ the mean collision rate, defined by the integral (5), diverges at the lower limit, i.e., the randomly accelerated inelastic particle makes an infinite number of collisions in a finite time. Cornell et al. [3] argued that even in the absence of a gravitational field this is the case.

The small v behavior (22), (23) is precisely the same as for a randomly accelerated particle moving on the finite line $0 < x < 1$ with inelastic collisions at $x = 0$ and 1 and with no gravitational field [4, 5]. In both cases the divergent behavior for $v \searrow 0$ comes from the high rate of low velocity inelastic collisions with one of the walls. For short times the diffusive change in velocity due to the random force, which grows as $t^{1/2}$, exceeds the change due to the gravitational force, which is proportional t . Thus, the random force is primarily responsible for the rapid return to the boundary and determines the small v behavior.

In both cases - the randomly accelerated particle on the half line with a gravitational field considered here, and on the finite line with no gravitational field considered in [5] - the distribution function $P(x, v)$ remains smooth, extended, and normalizable for $r < r_c$. In neither case does it collapse on the boundary. Thus, the infinite equilibrium collision rate does not lead to localization of the particle at the boundary.

B. Asymptotic form of $P(0, v)$ for large v

For large v one finds that the ansatz

$$P(0, v) \sim v^{-m(r)} e^{-q(r)v}, \quad v \rightarrow \infty. \quad (25)$$

is consistent with integral equation (17) with kernel (21) if the quantities $m(r)$ and $q(r)$ are chosen as follows: For $\frac{1}{2} \leq r < 1$,

$$m(r) = 1 - \frac{\ln r}{\ln[x(r)/r]}, \quad q(r) = \frac{3}{2} \frac{1-r}{1-r+r^2}, \quad (26)$$

where

$$x(r) = \frac{1}{2} + \frac{\sqrt{3}}{2} \frac{\frac{1}{2} - q}{\left[1 - \left(\frac{1}{2} - q\right)^2\right]^{1/2}}, \quad (27)$$

and for $r < \frac{1}{2}$,

$$m(r) = \frac{3}{2}, \quad q(r) = \frac{1}{2r}. \quad (28)$$

The functions $m(r)$ and $q(r)$ are shown in Figs. 1 and 2, respectively. As r decreases from 1 to $\frac{1}{2}$, $m(r)$ increases from 0 to 1 and then changes discontinuously to $\frac{3}{2}$ for $r < \frac{1}{2}$. As r decreases from 1 to 0, $q(r)$ increases monotonically from 0 to ∞ . The functional form of $q(r)$ changes at $r = \frac{1}{2}$, in accordance with Eqs. (26) and (28). Both q and dq/dr are continuous at $r = 1/2$, but d^2q/dr^2 is discontinuous.

The functions $m(r)$ and $q(r)$ are both non-analytic at $r = \frac{1}{2}$. Since they only characterize $P(0, v)$ in the large v limit (see Eq. (25)), it does not follow that $P(x, v)$ is non-analytic in r for fixed finite x and v . We have not found any indication of a phase transition, i.e., a non-analyticity of the distribution function $P(x, v)$, as r is varied with x and v fixed.

C. Exact $P(0, v)$ for $r = \frac{1}{2}$ and $\frac{1}{3}$

The curves for $\beta(r)$ and $m(r)$ in Fig. 1 cross at $r = \frac{1}{2}$ and $\frac{1}{3}$. For these two values of r , the exponents in the asymptotic forms (22) and (25) for small and large v are the same, with $\beta(\frac{1}{2}) = m(\frac{1}{2}) = 1$ and $\beta(\frac{1}{3}) = m(\frac{1}{3}) = \frac{3}{2}$. In fact, the functions

$$P(0, v) = \begin{cases} A_{1/2} v^{-1} e^{-v}, & r = \frac{1}{2}, \\ A_{1/3} v^{-3/2} e^{-3v/2}, & r = \frac{1}{3}, \end{cases} \quad (29)$$

turn out to be exact solutions of integral equation (17) for all $0 < v < \infty$, as we discovered numerically and prove analytically in Appendix B. The quantities $A_{1/2}$ and $A_{1/3}$ in Eq. (29) are normalization constants, which we now determine.

Substituting Eq. (29) in Eq. (16) and making use of Eqs. (9) and (14), we find that the corresponding $w(F)$ are given by

$$w(F) = \begin{cases} \frac{1}{2} A_{1/2} F^{-1/2} \exp [-(12F)^{-1}], & r = \frac{1}{2}, \\ \left(\frac{2}{27\pi}\right)^{1/2} A_{1/3} F^{-1/2} K_{1/6}((12F)^{-1}), & r = \frac{1}{3}, \end{cases} \quad (30)$$

where $K_\nu(z)$, as in Eq. (20), is a modified Bessel function. Together with Eq. (13), these $w(F)$ imply

$$A_{1/2} = \frac{1}{3}, \quad A_{1/3} = \left(\frac{27}{32\pi}\right)^{1/2} \quad (31)$$

for the normalization constants in Eqs. (29) and (30).

Combining Eqs. (12), (30), and (31), one obtains relatively simple expressions

$$P(x) = \begin{cases} \frac{1}{3} K_0(\sqrt{2x/3}) , & r = \frac{1}{2} , \\ \frac{1}{4\pi} \int_0^\infty dF F^{-1} K_{1/6}((12F)^{-1}) \exp[-(12F)^{-1} - Fx] , & r = \frac{1}{3} , \end{cases} \quad (32)$$

for the probability distribution of position. In the limit $x \rightarrow 0$, $P(x)$ diverges as $\log x$ and $x^{-1/6}$ for $r = \frac{1}{2}$ and $\frac{1}{3}$, respectively, and as $x^{(1-\beta)/3}$ for general r , as in Ref. [5]. In the limit $x \rightarrow \infty$, $P(x)$ decays as $x^{-1/4} \exp(-\sqrt{2x/3})$ and $x^{-1/2} \exp(-\sqrt{2x/3})$ for $r = \frac{1}{2}$ and $\frac{1}{3}$, respectively.

The distribution function $P(x, v)$ may be calculated numerically for $r = \frac{1}{2}$ and $\frac{1}{3}$ by combining Eqs. (7), (9), (30), and (31) and carrying out the integration over F numerically. The v dependence of $P(x, v)$ for $r = \frac{1}{2}$ and several values of x is shown in Fig. 3. For $r = \frac{1}{3}$ the curves are qualitatively similar. In both cases the curve for $x = 0$ diverges at $v = 0$, in accordance with Eqs. (22) and (23). For $x > 0$ the divergence is replaced by a smooth peak, which becomes lower and broader as x increases.

For large x the height of the peak in Fig. 3 varies as $P(x, 0) \sim x^{-1/2} \exp(-\sqrt{2x/3})$ for $r = \frac{1}{2}$ and as $P(x, 0) \sim x^{-3/4} \exp(-\sqrt{2x/3})$ for $r = \frac{1}{3}$. For small x , $P(x, 0) \sim x^{-1/3}$ and $x^{-1/2}$ for $r = \frac{1}{2}$ and $\frac{1}{3}$, respectively, and $P(x, 0) \sim x^{-\beta/3}$ for general r , as in Ref. [5].

The curves in Fig. 3 are characterized by the moments

$$\langle v^n \rangle_x = P(x)^{-1} \int_{-\infty}^{\infty} dv v^n P(x, v) , \quad (33)$$

where the normalizing denominator $P(x)$ is defined by Eq. (12). Taking the derivative of Eq. (33) with respect to x , making use of the Fokker-Planck equation (3), and integrating partially with respect to v , one finds that

$$\langle v \rangle_x = 0 , \quad (34)$$

$$\langle v^2 \rangle_x = P(x)^{-1} \int_x^\infty dx P(x) . \quad (35)$$

According to Eqs. (5), (33), and (34) the net probability current at a distance x from the boundary vanishes, as expected in equilibrium. Inserting the asymptotic form of $P(x)$, given just below Eq. (32), in Eq. (35), one finds that the root-mean-square width $\langle v^2 \rangle_x^{1/2}$ of the peak in Fig. 3 increases as $x^{1/4}$ in the large x limit, for both $r = \frac{1}{2}$ and $\frac{1}{3}$.

IV. SIMULATIONS

A. Algorithm

In our simulations the motion of the particle is governed by the difference equations

$$x_{n+1} = x_n + v_n \Delta_{n+1} - \frac{1}{2} \Delta_{n+1}^2 + \left(\frac{1}{6} \Delta_{n+1}^3 \right)^{1/2} (s_{n+1} + \sqrt{3} r_{n+1}) , \quad (36)$$

$$v_{n+1} = v_n - \Delta_{n+1} + (2\Delta_{n+1})^{1/2} r_{n+1} . \quad (37)$$

Here x_n and v_n are the position and velocity at time t_n , and $\Delta_{n+1} = t_{n+1} - t_n$. The quantities r_n and s_n are independent Gaussian random numbers with $\langle r_n \rangle = \langle s_n \rangle = 0$ and $\langle r_n^2 \rangle = \langle s_n^2 \rangle = 1$. This is the same as the algorithm in Refs. [8, 15], except that a gravitational field $g = 1$ has been included.

The algorithm (36), (37) is consistent with the exact probability distribution $P_g^{\text{free}}(x, v; x_0, v_0; t)$ in free space, i.e. in the absence of boundaries, of a randomly accelerated particle in a gravitational field $g = 1$ with initial conditions x_0, v_0 at $t = 0$. This quantity satisfies the time-dependent Fokker-Planck equation (A1) (see Appendix A) with initial condition (A2). The exact form of $P_g^{\text{free}}(x, v; x_0, v_0; t)$ follows immediately from Eq. (A4) and the expression for $P_0^{\text{free}}(x, v; x_0, v_0; t)$ in Eq. (27) of [15]

In free space there is no time-step error in the algorithm (36), (37). The time step Δ_{n+1} is arbitrary. However, for a particle on the half line $x > 0$, trajectories are not generated with the correct probability close to the boundary. This is because $P_g^{\text{free}}(x, v; x_0, v_0; t)$ includes trajectories which travel from positive to negative x and return during the time t , violating the restriction $x > 0$. As in Refs. [8, 15], we make the time step smaller near the boundary to exclude these spurious trajectories. Generalizing the discussion in Ref. [8] to include a gravitational field $g = 1$, we find that the spurious trajectories occur with negligible probability if the time step satisfies

$$x_n + v_n \Delta_{n+1} - \frac{1}{2} \Delta_{n+1}^2 - c \Delta_{n+1}^{3/2} > 0 , \quad (38)$$

where the constant c is about 5 or larger.

The most efficient time step is the largest Δ_{n+1} consistent with inequality (38), which we denote by $\mathcal{D}(x_n, v_n)$. Using a smaller time step slows the simulation without improving the accuracy. A convenient choice is $\Delta_{n+1} = \mathcal{D}(x_n, v_n) + \delta$, where a small minimum time step

has been included. Without it, the step size decreases to zero as the particle approaches the boundary, and it never gets there.

For small r the typical speed of the particle becomes extremely small after many boundary collisions. To simulate the behavior reliably, we reduced the minimum time step δ as the speed decreased, following Ref. [8]. After each boundary collision we set the root-mean square velocity change $\Delta v = (2\delta)^{1/2}$, corresponding to the minimum time step, equal to $1/500$ of the velocity just after the collision and then used this value of δ until the next boundary collision. This Δv is the smallest velocity the algorithm can handle reliably.

B. Results

According to Eq. (5) the equilibrium rate of boundary collisions in which the particle is reflected with velocity between v and $v + dv$ is given by $P(0, v) v dv$. We used this relation to determine $P(0, v)$ from our simulations.

In Fig. 4 the simulation results for $r = 0.75$ and $r = 0.25$ are compared with the exact asymptotic forms (22), (23) and (25)-(28) for small and large v , respectively. Varying the proportionality constants in Eqs. (22) and (25) shifts the dashed and solid curves vertically in the figure, without changing the slope. The proportionality constants were chosen to best fit the simulation data, and the fit is excellent.

In Fig. 5 the simulation results for $r = \frac{1}{2}$ and $r = \frac{1}{3}$ are compared with the exact analytical predictions (29) and (31). No adjustable parameters are involved. The agreement is excellent.

V. CONCLUDING REMARKS

In this paper we have studied the equilibrium of a particle on the half line subject to both a random force with zero mean and a constant gravitational force which drives the particle toward a single inelastic boundary. It is interesting to compare with the case [4, 5] of a randomly accelerated particle moving on the finite line between two inelastic boundaries with no gravitational field. In both cases the equilibrium distribution function has the same divergent behavior $P(0, v) \sim v^{-\beta}$ for small v , given in Eqs. (22), (23). As discussed below Eq. (24), this comes from a high rate of low velocity inelastic collisions with one of the

boundaries. In both cases the random force, not gravity, is responsible for the rapid return of a low velocity particle to the boundary.

In contrast, the equilibrium behavior for high velocities is different in the two cases. With a single boundary and a gravitational field, $P(0, v) \sim v^{-m} e^{-qv}$ for large v , according to Eqs. (25)-(28). With two boundaries and no gravitation, $P(0, v) \sim \exp[-(v/v_{\text{ch}})^3]$, according to Eqs. (14) and (16) of Ref. [5]. Thus, in the case of two boundaries high velocities are far more strongly suppressed. This is not surprising. Since a high velocity particle quickly travels between the two boundaries with negligible change in velocity, the time between inelastic collisions decreases as $|v|^{-1}$ as $|v|$ increases. In the case of a single boundary and a gravitational field, on the other hand, a particle which leaves the boundary with a high velocity travels far from the boundary before it returns, and the mean time between the inelastic collisions increases linearly with $|v|$.

We conclude with quantitative answers to some simple questions one might ask on reading the title of the paper: What is the mean height $\langle x \rangle$ of the ball above the inelastically reflecting surface, how large is the root-mean-square fluctuation $\Delta x = \langle (x - \langle x \rangle)^2 \rangle^{1/2}$, and what is the equilibrium collision rate I ? In the two cases $r = \frac{1}{2}$ and $\frac{1}{3}$ where we have found the exact equilibrium distribution function $P(x, v)$, Eqs. (5), (29), (31), and (32) imply

$$\begin{aligned} r = \frac{1}{2} : \quad \langle x \rangle &= 6, & \Delta x &= 10.4, & I &= \frac{1}{3}, \\ r = \frac{1}{3} : \quad \langle x \rangle &= 3.89, & \Delta x &= 7.68, & I &= \frac{3}{4}, \end{aligned} \tag{39}$$

For both values of r the fluctuations in the height of the ball are larger than the mean height. For $r = \frac{1}{3}$, the mean height is smaller and the collision rate is larger than for $r = \frac{1}{2}$. The mean height is expected to decrease as r decreases but remain positive for all $0 < r < 1$, since $P(x)$ remains positive and integrable. The collision rate is expected to increase as r decreases and is infinite for $r < r_c$, as discussed below Eq. (24). Finally, we note that these results for $g = \Lambda = 1$ in Eq. (39) are easily generalized to arbitrary values of the parameters g and Λ in Eq. (1). In accordance with footnote [1], the numerical values in Eq. (39) for $\langle x \rangle$ and Δx are multiplied by $g^{-3}\Lambda^2$ and for I by $g^2\Lambda^{-1}$.

Acknowledgments

TWB thanks Dieter Forster for very informative conversations about the function $K_{i\gamma}(v)$.

APPENDIX A: ALTERNATE EXPRESSIONS FOR $G_g(v, u)$

To discuss first-passage properties, we define $P_g(x, v; x_0, v_0; t)dx dv$ as the probability that the position and velocity of a particle, moving on the half line $x > 0$ according to Eq. (1) with $g = \Lambda = 1$, have evolved from x_0, v_0 to values between x and $x + dx$, v and $v + dv$ in a time t without ever reaching $x = 0$. The quantity P_g satisfies the time-dependent Fokker-Planck equation [9]

$$\left(\frac{\partial}{\partial t} + v \frac{\partial}{\partial x} - \frac{\partial}{\partial v} - \frac{\partial^2}{\partial v^2} \right) P_g(x, v; x_0, v_0; t) = 0, \quad (\text{A1})$$

with the initial condition

$$P_g(x, v; x_0, v_0; 0) = \delta(x - x_0)\delta(v - v_0) \quad (\text{A2})$$

and the absorbing boundary condition

$$P_g(0, v; x_0, v_0; t) = 0, \quad v > 0. \quad (\text{A3})$$

In the absence of the gravitational field, i.e. in the case $g = 0$ instead of $g = 1$, the corresponding probability distribution $P_0(x, v; x_0, v_0; t)$ satisfies the same Fokker-Planck equation, boundary condition, and initial condition, except that the third term $-\partial P/\partial v$ in Eq. (A1) is absent. This leads to the simple relation

$$P_g(x, v; x_0, v_0; t) = e^{-(v-v_0)/2-t/4} P_0(x, v; x_0, v_0; t) \quad (\text{A4})$$

between the distribution functions with and without gravity.

As discussed below Eq. (18), the quantity $vG_g(v, u)dv$ in integral equation (17) represents the probability that a particle moving according to Eq. (1) with initial position $x = 0$ and initial velocity $u > 0$ arrives with speed between v and $v + dv$ on its first return to $x = 0$. Since the return occurs between t and $t + dt$ with probability $vP_g(0, -v; 0, u; t) dv dt$,

$$G_g(v, u) = \int_0^\infty dt P_g(0, -v; 0, u; t) = e^{(v+u)/2} \tilde{P}_0(0, -v; 0, u; \tfrac{1}{4}), \quad (\text{A5})$$

where we have made use of Eq. (A4) and introduced the Laplace transform

$$\tilde{P}_0(x, v; x_0, v_0; s) = \int_0^\infty dt e^{-st} P_0(x, v; x_0, v_0; t). \quad (\text{A6})$$

In a classic paper on the first passage properties of a randomly accelerated particle, McKean [13] derived the exact form of $P_0(0, -v; 0, u; t)$ and its Laplace transform. The expressions for $G_g(v, u)$ in Eqs. (20) and (21) follow from Eq. (A5) and McKean's Eqs. (5) and (6).

APPENDIX B: DERIVATION OF EXACT $P(0, v)$ FOR $r = \frac{1}{2}$ AND $\frac{1}{3}$

Expression (20) for $G_g(v, u)$ and the Kontorovich-Lebedev transforms [16]

$$f(v) = \int_0^\infty d\gamma g(\gamma) K_{i\gamma}(v) , \quad (\text{B1})$$

$$g(\gamma) = 2\pi^{-2}\gamma \sinh(\pi\gamma) \int_0^\infty dv v^{-1} f(v) K_{i\gamma}(v), \quad (\text{B2})$$

imply

$$v^{-1}e^{v/2} K_{i\gamma}(v) = 2 \cosh\left(\frac{\pi\gamma}{3}\right) \int_0^\infty du G_g(v, u) e^{-u/2} K_{i\gamma}(u) . \quad (\text{B3})$$

For $i\gamma \rightarrow \frac{1}{2}$, $K_{i\gamma}(v) \rightarrow \text{const} \times v^{-1/2}e^{-v}$, and integral equation (B3) is entirely equivalent to Eq. (17), with $r = \frac{1}{3}$ and $P(0, v) \propto v^{-3/2}e^{-3v/2}$. Thus, we have found the exact $P(0, v)$ for $r = \frac{1}{3}$, already announced in Eq. (29).

The other result in Eq. (29), that $P(0, v) \propto v^{-1}e^{-v}$ for $r = \frac{1}{2}$ is an exact solution of the integral equation (17), is readily proved by integrating Eq. (B3) over γ from $\gamma = 0$ to ∞ and then using the results,

$$\int_0^\infty d\gamma K_{i\gamma}(v) = \frac{\pi}{2} e^{-v} , \quad (\text{B4})$$

$$\int_0^\infty d\gamma \cosh\left(\frac{\pi\gamma}{3}\right) K_{i\gamma}(v) = \frac{\pi}{2} e^{-v/2} . \quad (\text{B5})$$

These relations, which are examples of the Kontorovich-Lebedev transforms (B1), (B2), follow directly from Ref. [14], Eq. (6.795-1).

-
- [1] In terms of the dimensionless variables $\xi = g^3 \Lambda^{-2} x$, $\tau = g^2 \Lambda^{-1} t$, Eq. (1) takes the form $d^2 \xi / d\tau^2 = -1 + \zeta(\tau)$, $\langle \zeta(\tau) \zeta(\tau') \rangle = 2\delta(\tau - \tau')$.
 - [2] S. J. Moon, J. B. Swift, and H. L. Swinney, Phys. Rev. E **69**, 011301 (2004).
 - [3] S. J. Cornell, M. R. Swift, A. J. Bray, Phys. Rev. Lett. **81**, 1142 (1998).
 - [4] T. W. Burkhardt, J. Franklin, and R. R. Gawronski, Phys. Rev. E **61**, 2376 (2000).
 - [5] T. W. Burkhardt and S. N. Kotsev, Phys. Rev. E **70**, 026105 (2004).
 - [6] T. W. Burkhardt, J. Phys. A **26**, L1157 (1993).
 - [7] T. W. Burkhardt, J. Phys. A **33**, L429 (2000); G. De Smedt, C. Godrèche, and J. M. Luck, Europhys. Lett. **53**, 438 (2001).
 - [8] S. N. Kotsev and T. W. Burkhardt, Phys. Rev. E **71**, 046115 (2005).
 - [9] See, e.g., S. Chandrasekhar, Rev. Mod. Phys. **15**, 1 (1943); *Statistical Mechanics*, D. A. McQuarrie (Harper & Row, New York, 1976).
 - [10] *Handbook of Mathematical Functions*, edited by M. Abramowitz and I. A. Stegun (Dover, New York, 1965).
 - [11] T. W. Marshall and E. J. Watson, J. Phys A **18**, 3531 (1985).
 - [12] A. J. Kainz and U. M. Titulaer, J. Phys. A **24**, 4677 (1991).
 - [13] H. P. McKean, J. Math. Kyoto Univ. **2**, 227 (1963).
 - [14] I. S. Gradshteyn and I. M. Ryzhik, *Tables of Integrals, Series, and Products* (Academic, New York, 1980).
 - [15] D. J. Bicout and T. W. Burkhardt, J. Phys. A **33**, 6835 (2000).
 - [16] *Tables of Integral Transforms*, Bateman Manuscript Project, Vol 2, edited by A. Erdélyi (McGraw-Hill, New York, 1954).

Figure Captions

Figure 1: The exponents $m(r)$ and $\beta(r)$, given by Eqs. (22), (23), and (25)-(28). Note the discontinuity in $m(r)$ at $r = \frac{1}{2}$.

Figure 2: The decay constant $q(r)$, given by Eqs. (26) and (28). Both $q(r)$ and $dq(r)/dr$ are continuous at $r = \frac{1}{2}$, but d^2q/dr^2 is discontinuous.

Figure 3: Exact $P(x, v)$, given by Eqs. (7), (9), (30), and (31), for $r = \frac{1}{2}$ and, from top to bottom, $x = 0, 0.001, 0.01$, and 0.1 .

Figure 4: Double-logarithmic plot (base 10) of $P(0, v)$ for $r = 0.75$ and 0.25 . The points are the results of our simulations. The dashed and solid lines show the predicted asymptotic forms (22), (23) for small v and (25)-(28) for large v , respectively, with proportionality constants chosen to fit the simulation data.

Figure 5: Double-logarithmic plot (base 10) of $P(0, v)$ for $r = \frac{1}{2}$ and $\frac{1}{3}$. The points are the results of our simulations. The solid curves show the exact theoretical predictions (29) and (31), with no adjustable parameters.

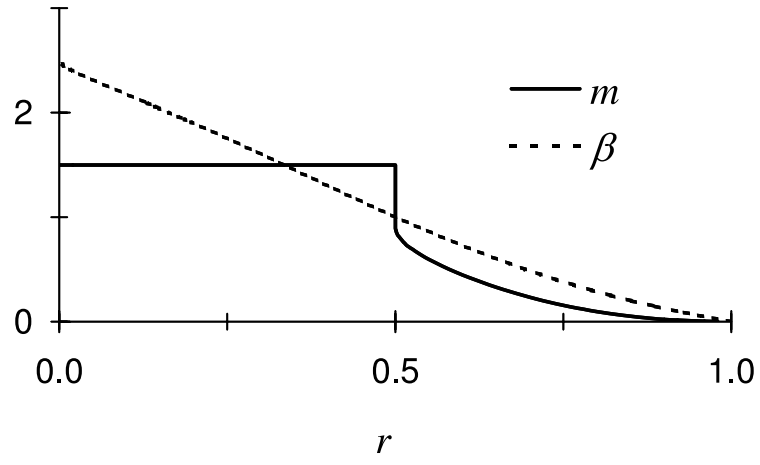


FIG. 1: The exponents $m(r)$ and $\beta(r)$, given by Eqs. (22), (23), and (25)-(28). Note the discontinuity in $m(r)$ at $r = \frac{1}{2}$.

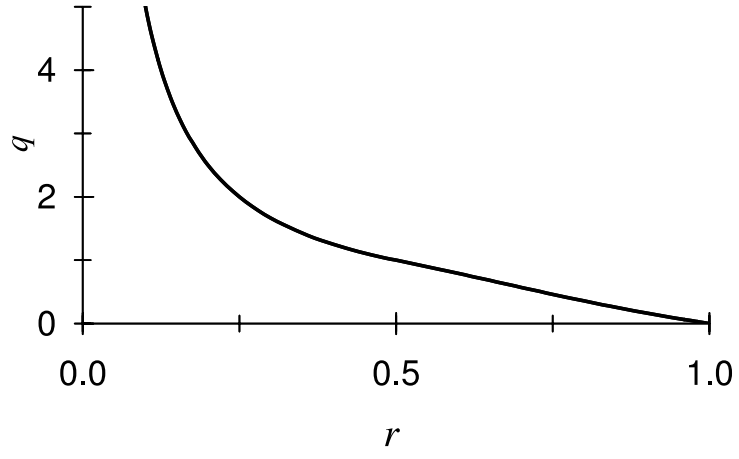


FIG. 2: The decay constant $q(r)$, given by Eqs. (26) and (28). Both $q(r)$ and $dq(r)/dr$ are continuous at $r = \frac{1}{2}$, but d^2q/dr^2 is discontinuous.

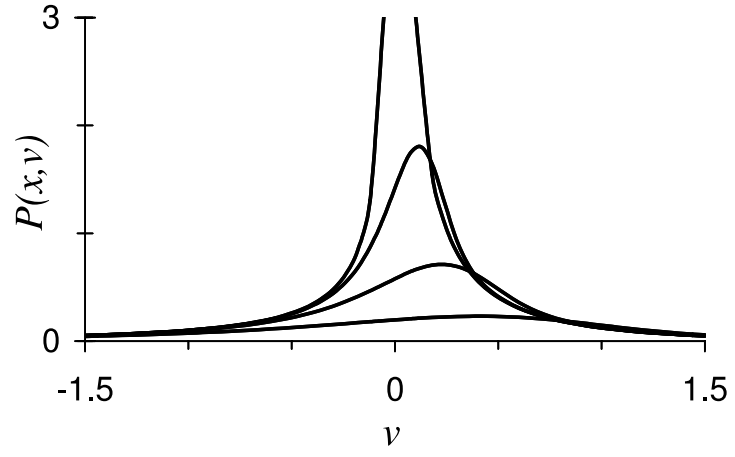


FIG. 3: Exact $P(x, v)$, given by Eqs. (7), (9), (30), and (31), for $r = \frac{1}{2}$ and, from top to bottom, $x = 0, 0.001, 0.01$, and 0.1 .

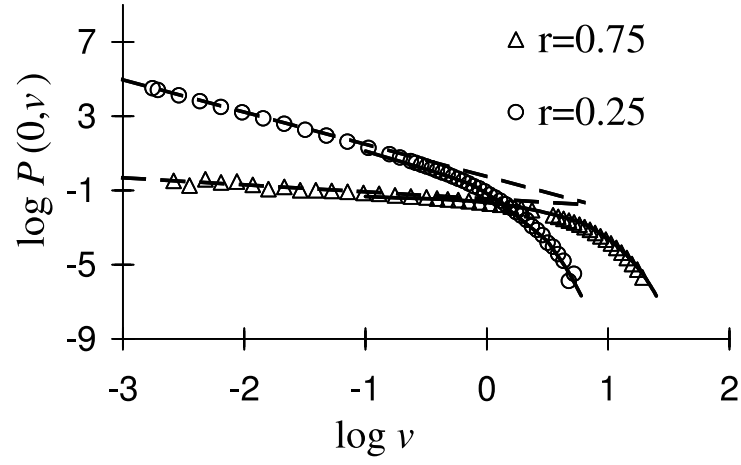


FIG. 4: Double-logarithmic plot (base 10) of $P(0, v)$ for $r = 0.75$ and 0.25 . The points are the results of our simulations. The dashed and solid lines show the predicted asymptotic forms (22), (23) for small v and (25)-(28) for large v , respectively, with proportionality constants chosen to fit the simulation data.

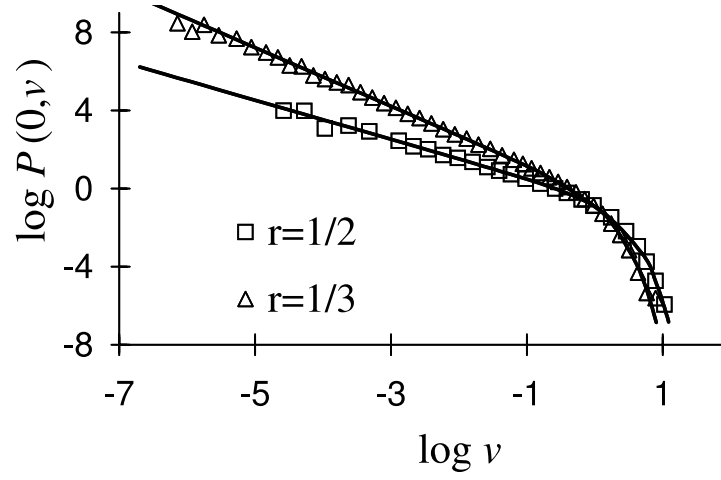


FIG. 5: Double-logarithmic plot (base 10) of $P(0, v)$ for $r = \frac{1}{2}$ and $\frac{1}{3}$. The points are the results of our simulations. The solid curves show the exact theoretical predictions (29) and (31), with no adjustable parameters.